12th AIAA/CEAS Aeroacoustics Conference (27th AIAA Aeroacoustics Conference)
8 - 10 May 2006, Cambridge, Massachusetts

AIAA 2006-2590

Superdirective acoustic radiation by vortex pairing in subsonic excited jets

Vincent Fleury*, Christophe Bailly† and Daniel Juvé‡
Laboratoire de Mécanique des Fluides et d'Acoustique
UMR CNRS 5509 & Ecole Centrale de Lyon
69134 Ecully, France

This paper is concerned with acoustic radiation of the first subharmonic of the forcing frequency in a low-Mach-number excited jet. Two jets with laminar and transitional initial conditions are experimentally studied in the same facility. An acoustic directivity with an extinction angle in the sideline direction is observed for the laminar case ($\mathrm{Re}_D = 6.7 \times 10^4$), that can be interpreted as the radiation of a compact axisymmetric quadrupolar source. A superdirective radiation is measured for the transitional jet ($\mathrm{Re}_D = 1.3 \times 10^5$), that is characterized by an exponential angular variation providing a larger range of the sound pressure level. A wave extrapolation method is developed to interpret the measured near and far pressure fields of these two configurations.

I. Introduction

Mollo-Christensen[1] *et al.* was one of the first study to stress the importance of organized structures in jet noise. A large number of works were subsequently devoted to the investigation of the role of coherent structures in the jet flow, and especially at the end of the potential core. Thanks to a coherent external acoustic excitation, Crow & Champagne[2] were able to organize and enhance the growth of centerline fluctuations and thus revealed the presence of a preferred mode, the jet column mode. The Strouhal number St_D of this mode is in close relation with the Strouhal number of the hump in the far field pressure spectra, $\mathrm{St}_D \simeq 0.3$, the exact value depending on the observation angle. The Strouhal number is defined by $\mathrm{St}_D = fD/U_j$ where f is the frequency, D is the jet diameter and U_j is the jet exit velocity. Crow & Champagne[2] also investigated the structure of the jet column mode and exhibited large-scale vortex puffs for jets at Reynolds numbers $\mathrm{Re}_D = U_j D/\nu$ between 10^3 and 10^4, where ν is the kinematic viscosity. Laufer[3] suggested that the pairing of vortical structures is a pre-eminent noise mechanism in subsonic jets. Although the coherent process of pairing was quickly recognized to be very unlikely in natural jets, this noise source has been much studied as it constitutes a benchmark for the application of aeroacoustic analogies[4–6] and for the comparison of basic noise theories.[7–9]

In a jet with a laminar initial shear-layer, stable pairing is usually obtained for a suitable excitation.[10,11] Kibens,[10] for instance, obtained a stable cascade of three successive pairing stages by controlling the growth of the most unstable shear-layer mode predicted by the linear stability theory.[12,13] Pairings occurred at fixed positions and generated discrete noise components, *e.g.* the first subharmonic of the excitation frequency, $f_{s1} = f_{ex}/2$, which is associated to the first pairing, and the second and third subharmonics, $f_{s2} = f_{ex}/4$ and $f_{s3} = f_{ex}/8$, corresponding to the second and third pairing stages respectively. Bridges & Hussain[14] performed a careful investigation of the acoustic radiation produced by stable pairing in a similar laminar low-Mach-number jet at $\mathrm{Re}_D = 7.4 \times 10^4$ and noticed an extinction angle $\theta^\star$ in the acoustic far field, at 65° from the jet axis in the downstream direction. This cancellation was explained[14] by modeling the aerodynamic noise source by an axisymmetric and compact distribution of quadrupolar source terms. Such a description

*Ph.D. student
†Professor, corresponding author: christophe.bailly@ec-lyon.fr, Senior Member AIAA.
‡Professor, Senior Member AIAA.

indeed predicts[15,16] an extinction angle $\theta^\star$ around 55°. Several assumptions have been put forward to explain the discrepancy between this theoretical value and measurements[8] or numerical simulations.[4]

Laufer & Yen[17] also investigated vortex pairing noise in low-Mach-number jets but at higher Reynolds numbers ($\mathrm{Re}_D > 10^5$) than in Bridges & Hussain,[14] so that the conditions of the initial shear-layer were probably not fully laminar. From the classification established by Zaman,[18] the initial flow state is suspected to have been *nominally laminar* in this case. The measured acoustic directivity[17] is radically different from the observations of Bridges & Hussain.[14] In particular, there is no extinction angle, and the directivity is oriented far more in the downstream direction. An exponential antenna factor, qualified as superdirective,[19] was proposed by Laufer & Yen[17] to mimic this distribution. This puzzling result was addressed theoretically by Huerre & Crighton,[7] who argued that such an exponential radiation diagram cannot result from a compact source in spite of the very low Mach number of the jet. They therefore developed Lighthill's analogy[20] for a non-compact source in the axial direction, and recovered a similar superdirective antenna factor for a Gaussian distribution of the source term along the shear-layer. Some discrepancies remain however between the predicted acoustic field and the measurements. An alternative approach based on a wavy-wall analogy was later proposed by Crighton & Huerre.[19] Instead of modeling the aeroacoustic source term of the vortex pairing, these authors considered the streamwise distribution of pressure slightly outside the shear-layer and calculated the pressure radiated from this boundary by resolving a wave equation outside the jet. From a Gaussian wave-like distribution, the exponential antenna factor was again recovered.

Motivation and goals

The present work brings further insight into the noise mechanisms associated to vortex pairing in low-Mach-number excited jets, and reports a new experimental evidence of the superdirective radiation backing up the work of Laufer & Yen.[17] Note also that to the best of our knowledge, no other experimental work has been published since the work of Bridges & Hussain[14] to investigate the directivity and the location of the extinction angle in excited jets. In the present work, the two radiation patterns were recovered in the same facility to avoid usual criticisms, such as a possible artefact introduced by the nozzle in the Laufer & Yen experiment.[17]

The initial conditions are suspected to play a key role. The streamwise dynamics of vortices is indeed strongly controlled by the state of the boundary-layer at the nozzle exit,[21] which probably influences the emitted acoustic radiation. Two jets were investigated, one with a laminar initial shear-layer and the other with transitional initial conditions. The same experimental facility was used in both cases and only the jet velocity U_j was varied. An external acoustic excitation was used to control the natural axisymmetric instability wave in the shear-layer and thus to enhance the pairing process, following Zaman & Hussain.[11] The two radiation patterns of the vortex pairing were reproduced. For the two configurations, flow properties are carefully documented and characterized to highlight the specific noise mechanisms.

The paper is structured as follows. The experimental procedure as well as the initial flow conditions for the two jets are presented in § 2. Experimental results are reported in § 3 for flow characteristics under forcing and the acoustic radiation of the first subharmonic. These experimental results are analysed in § 4 thanks to a wave extrapolation method developed in Appendix A. A discussion and some concluding remarks are given in § 5.

II. Jet facility and data processing

The experiments were performed with a circular jet of diameter $D = 5$ cm and for two velocities U_j, 20 m.s^{-1} and 40 m.s^{-1}, corresponding to Reynolds numbers Re_D of 6.7×10^4 and 1.3×10^5 respectively. The experiments were carried out in the small anechoic wind tunnel ($6.10 \times 4.60 \times 3.80$ m^3, cut-off frequency 100 Hz) of the Centre Acoustique located at Ecole centrale de Lyon.[22] The flow was powered by a variable velocity fan and conditioned by mufflers, mesh screens and honeycombs down to the converging nozzle of area ratio 1/46. The turbulence level in the jet at the nozzle exit was less than 0.3 %, and the jet velocity U_j varied by less than 1 % during the experiments. An excitation device constituted by four loudspeakers and cavities enabled to control the shear-layer at the nozzle exit. The acoustic perturbation was generated through a 2 mm-wide slot oriented at $\theta = 110^\circ$ from the jet axis. The nozzle including the speakers was designed to minimize possible acoustic reflexions and to prevent possible feedback. Note also that the nozzle

is not baffled, in contrast to the experiments of Laufer & Yen.[17]

Velocity measurements were made with a 5 μm diameter and 1.25 mm long hot-wire mounted on a Dantec Streamline constant temperature anemometer. The overheat ratio was 0.80 and the frequency response was optimized up to 20 kHz, which is sufficient for the present work. The near pressure field was investigated with a 1/8″ Bruel & Kjaer (BK) microphone and the acoustic far-field with a 1/2″ BK microphone. Velocity and pressure spectra, denoted by u'_f (m.s^{-1}) and p'_f (Pa) respectively, were measured by a Hewlett-Packard 35652B analyser with a frequency resolution of 8 Hz, and 1000 data blocks were used to compute the power spectral density.

Figures 1(a) and 1(b) display the velocity profiles for the natural jet at two axial locations. Near the nozzle exit, the mean velocity profiles are in good agreement with the Blasius profile, as shown in Figure 1(a), with a shape factor close to 2.56. Velocity profiles measured at $x/D \simeq 0.09$ are also plotted in Figure 1(b). The mean axial velocity profiles are well approximated by a hyperbolic tangent profile. Note that streamwise velocity fluctuations grow by an order of magnitude as U_j increases. This is attributed to a Reynolds number effect. Following Zaman's classification,[18] the boundary-layer is laminar at $U_j = 20$ m.s^{-1} and nominally laminar at 40 m.s^{-1}. Turbulence levels, as well as other initial flow characteristics, are reported in Table 1. The natural development of the two jets was also investigated and data can be found in Fleury.[23]

Boundary-layer			
U_j	δ_θ/D	u'_M/U_j	H
20 m.s^{-1}	0.0023	0.14 %	2.62
40 m.s^{-1}	0.0026	3.34 %	2.53

Shear-layer				
U_j	δ_θ/D	u'_M/U_j	f_0 ($St_{\delta_{\theta_0}}$)	f_1 ($St_{\delta_{\theta_1}}$)
20 m.s^{-1}	0.0042	0.18 %	1283 Hz (0.0135)	1520 Hz (0.0160)
40 m.s^{-1}	0.0028	3.36 %	4144 Hz (0.0144)	4950 Hz (0.0172)

Table 1. Initial flow characteristics in the boundary-layer and in the shear-layer. δ_θ is the momentum thickness, u'_M is the maximum velocity fluctuation at $r = r_{1/2}$ in the boundary layer, with $r_{1/2}$ defined as $U(r = r_{1/2}) = U_j/2$, or the shear-layer centre ($r = D/2$), and H is the shape factor. The frequencies f_0 and f_1 are associated to the natural axisymmetric and first helical shear-layer modes respectively.

III. Experimental results

The excitation device was used to control the development of the natural axisymmetric disturbance in the shear-layer and therefore, to organize vortex pairing. Freymuth[13] and Michalke[12] demonstrated the broadband frequency receptivity of the shear-layer and exhibited a maximum growth rate of the fluctuation $u'_{f_{ex}}$ for an excitation Strouhal number $\mathrm{St}_{\delta_{\theta ex}}$ around 0.017.

The excitation frequency f_{ex} and the excitation level $a_{f_{ex}}$ are reported in Table 2 for the two jet velocities. For comparison, Husain & Hussain[24] used excitation levels $a_{f_{ex}}$ and $a_{f_{ex}/2}$ of 0.1 % to force a laminar shear-layer. Laufer & Yen[17] mentioned the maximum saturation of $u'_{f_{ex}}/U_j$ along the shear-layer. A fluctuation rate between 2% to 7.6% was measured, which is slightly lower than the levels used in the present study, namely 7.5% for $U_j = 20$ m.s^{-1} and 11% for $U_j = 40$ m.s^{-1}. This difference results mainly from the high excitation Strouhal number $\mathrm{St}_{\delta_\theta}(f_{ex})$ used by these authors, around 0.017 instead of the optimal value[11] of 0.012.

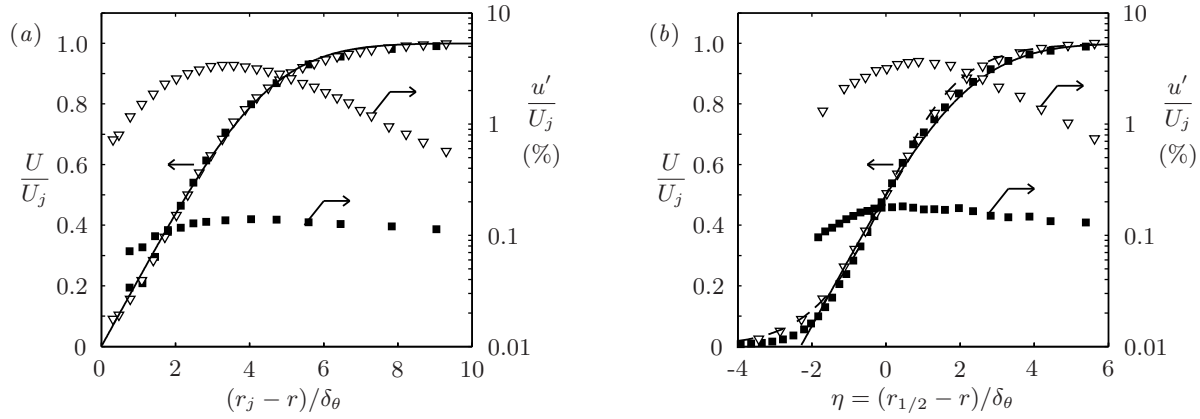

Figure 1. Mean and fluctuating velocity profiles for the two velocities ■ : $U_j = 20$ m.s^{-1} and ▽ : $U_j = 40$ m.s^{-1}. Figure (a) shows the boundary layer profiles measured at $x = 0.5$ mm from the nozzle exit, The Blasius profile is plotted in solid line —— and $r_j = D/2$ is the initial jet radius. Figure (b) shows the shear-layer profiles measured at $x = 3.5$ mm from the nozzle exit, where $r_{1/2}$ is defined as $U(r = r_{1/2}) = U_j/2$. The dashed curve - - - represents the hyperbolic tangent mean profile $U/U_j = 0.5\,[1 + \tanh(\eta)]$.

U_j	Re_D	M	f_{ex} (St_{δ_θ})	$a_{f_{ex}}$
20 m.s^{-1}	6.7×10^4	0.06	1500 Hz (0.0158)	0.05 %
40 m.s^{-1}	1.3×10^5	0.12	3530 Hz (0.0124)	0.1 %

Table 2. Excitation characteristics.

A. Jet characteristics under forcing

Times traces and spectral analysis

To analyse the influence of the excitation on the stability of the vortex pairing, velocity time traces and spectra were measured in the shear-layer and in the potential core. For $U_j = 20$ m.s^{-1}, shear-layer fluctuations are quasi-periodic and well organized according to the frequency f_{ex} and its first two subharmonics f_{s1} and f_{s2} as shown in Figures 2(a) and 2(b). This indicates the presence of a stable vortex pairing cascade with at least two successive pairings in the shear-layer. A third pairing is also detected in the potential core. Centreline fluctuation spectra shown in figure 2(c) indicate indeed the presence of a third subharmonic $f_{s3} = f_{ex}/8$. This coherent low-frequency fluctuation controls the jet column mode by imposing its Strouhal number $\mathrm{St}_D(f_{s3})$ close to 0.47. In this case, both centreline and shear-layer fluctuations are synchronized by the excitation.

For $U_j = 40$ m.s^{-1}, shear-layer fluctuations are clearly much less organized, as reported in Figure 3(a). The spectrum in Figure 3(b) reveals the suppression of the second subharmonic $u'_{f_{s2}}$ and therefore the absence of a coherent second pairing stage in the shear-layer. As in the natural jet (not reported here), the pairing cascade is inhibited by the breakdown of vortices during the first pairing, which is the main difference with the laminar shear-layer. Close to the nozzle exit, centreline fluctuations are controlled by the fluctuations associated to the excitation and the first subharmonic, see Figure 3(c), but farther downstream the spectral energy of velocity fluctuations is broadband as in the natural jet. The presence of the second subharmonic $u'_{f_{s2}}$ probably results from a few stable vortices, which do not break down during the first pairing stage, and thus generate a second subharmonic through their interaction. This contribution of $u'_{f_{s2}}$ is however weak and was not detected in the shear-layer. In the present case, the effects of the excitation are limited to the initial development of the jet, and the flow is turbulent downstream of the pairing–breakdown position.

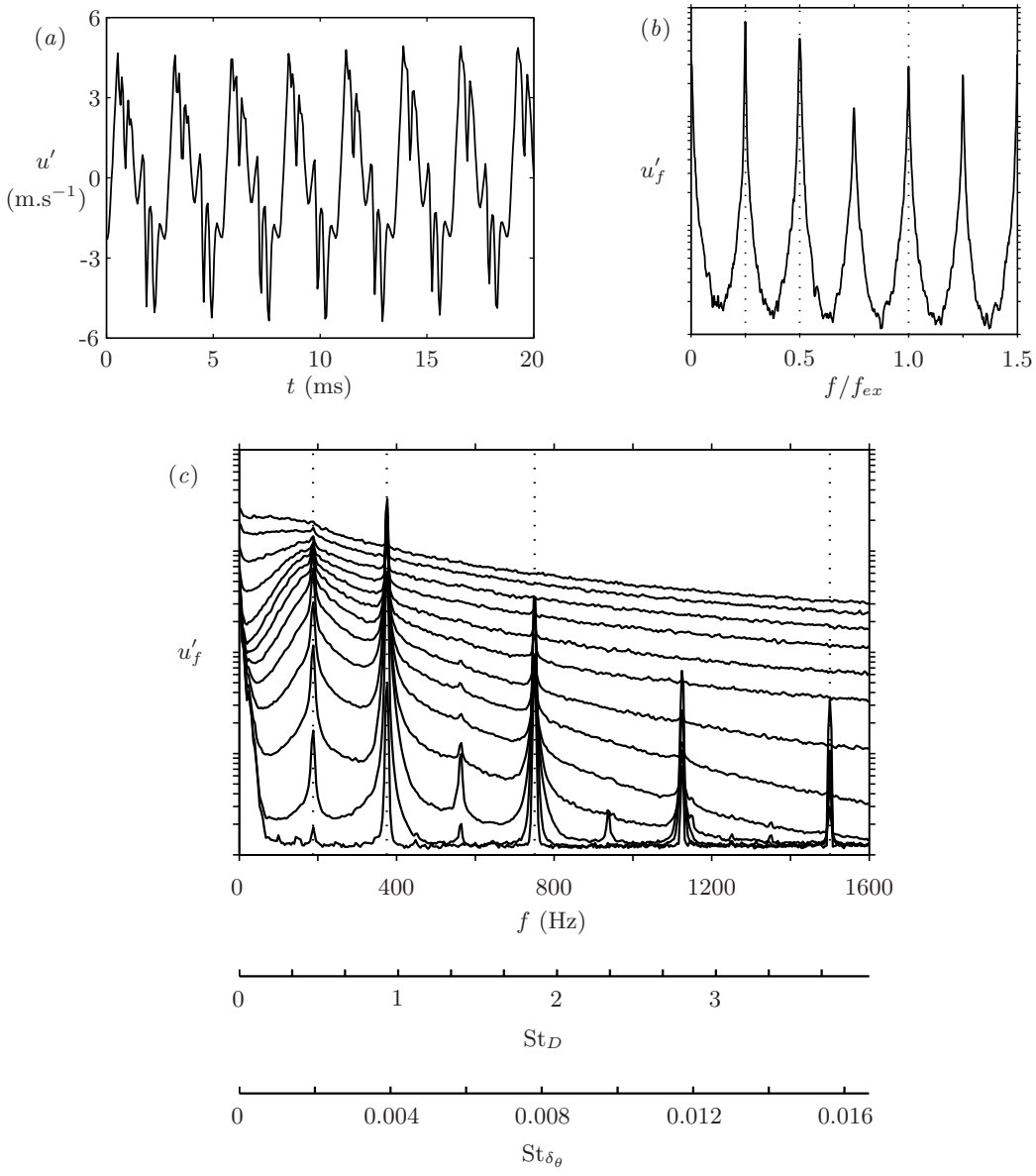

Figure 2. Velocity fluctuations for the excited jet at $U_j = 20$ m.s^{-1}. A typical velocity signal measured in the shear-layer at $x = D/2$ is shown (a) and its PSD is given in (b). Centreline velocity spectra are plotted in figure (c), from $x = 0$ (bottom) to $x = 6D$ (top), every $\Delta x = D/2$. The dotted lines ····· indicate the excitation frequency f_{ex} and its first three subharmonics f_{s1}, f_{s2} and f_{s3}.

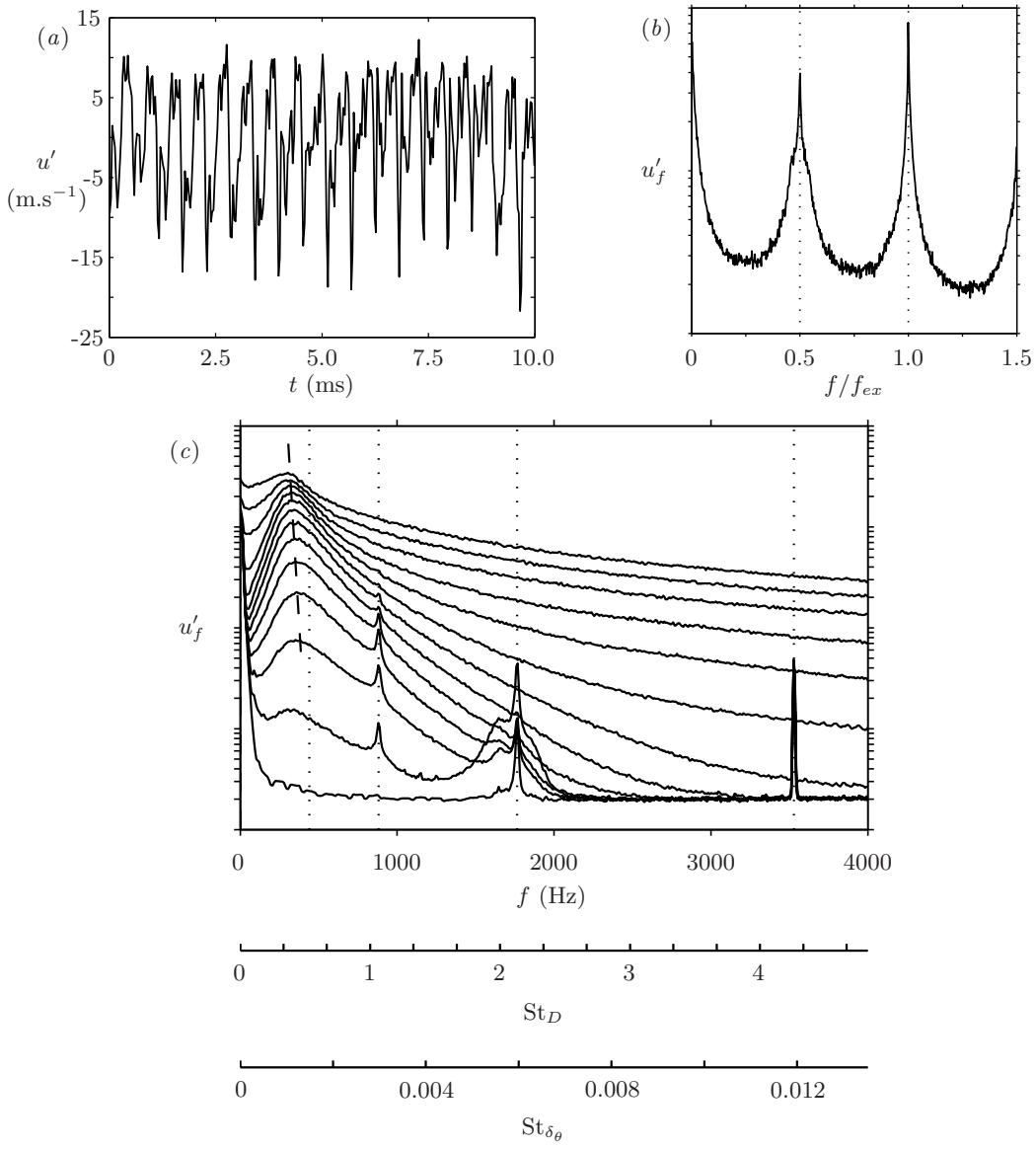

Figure 3. Velocity fluctuations for the excited jet at $U_j = 40$ m.s^{-1}. The legend is the same as in Figure 2. The dashed line – – – in (c) indicates the jet column mode.

Growth of the fundamental and the subharmonics in the shear-layer

The initial growth of the shear-layer fluctuations $u'_{f_{ex}}$, $u'_{f_{s1}}$ and, for $U_j = 20$ m.s^{-1}, $u'_{f_{s2}}$, is well predicted by the linear stability theory, but farther downstream, as their amplitude reaches higher levels, non-linear interactions are expected. Therefore, the presence or not of the second subharmonic influences the dynamics of $u'_{f_{ex}}$ and $u'_{f_{s1}}$. This point is considered in the present section.

For $U_j = 20$ m.s^{-1}, the streamwise dynamics of $u'_{f_{ex}}$, $u'_{f_{s1}}$ and $u'_{f_{s2}}$ are shown in figure 4(a). Initially, the growth is exponential and is faster for higher Strouhal numbers St_{δ_θ}, as predicted by the linear stability theory for $St_{\delta_\theta} < 0.017$. The decrease of the growth rate of $u'_{f_{s1}}$, which is observed at $x = 0.14D = 33\delta_\theta$, results from the non-linear resonant interaction with $u'_{f_{ex}}$. The growth of $u'_{f_{s1}}$ is reinitiated farther downstream by the saturation of $u'_{f_{ex}}$ in $x_{ex} = 0.22D = 52\delta_\theta$ with a turbulent rate $u'_{f_{ex}}/U_j$ of 6%. For a turbulent intensity $u'_{f_{s1}}/U_j$ of 2%, a resonant interaction occurs with the second subharmonic $u'_{f_{s2}}$, resulting in this case in a reduction of $u'_{f_{s2}}$ around $x = 0.26D = 62\delta_\theta$. A similar mechanism of attenuation was observed by Husain & Hussain[24] when the Strouhal number St_{δ_θ} of the dominant disturbance is lower than 0.01. In the present interaction, the dominant fluctuation is $u'_{f_{s1}}$ with a Strouhal number of 0.008. This first subharmonic $u'_{f_{s1}}$ then grows up to $x_{s1} \simeq 2x_{ex}$, where it saturates with a turbulent rate of around 16.5%. As defined by Ho & Huang,[26] the saturation of the first subharmonic corresponds to the position of the first vortex pairing, where the maximum of acoustic pressure is generated during the pairing process. The saturation of $u'_{f_{s1}}$ is accompanied by a transfer of energy in favour of $f_{ex} = 2f_{s1}$. The same mechanism is observed during the second pairing stage in $x_{s2} \simeq 4x_{ex}$, whence energy is then supplied to $u'_{2\times f_{s2}=f_{s1}}$ by the distortion of the velocity fluctuation $u'_{f_{s2}}$. The first subharmonic $u'_{f_{s1}}$ displays thus two humps along the shear-layer. Though not well documented, this phenomenon can be also noticed in the data presented by Laufer & Zhang[27] in their figure 40.

For $U_j = 40$ m.s^{-1}, the streamwise evolution of $u'_{f_{ex}}$ and $u'_{f_{s1}}$ is less complex, since the second subharmonic is not involved. As shown in figure 4(b), the disturbance $u'_{f_{ex}}$ saturates in $x_{ex} = 0.16D = 57\delta_\theta$ for $u'_{f_{ex}}/U_j = 11\%$. A second maximum of $u'_{f_{ex}}$ is noticed at $x = x_{s1} = 0.5D = 179\delta_\theta$, where $u'_{f_{s1}}$ saturates, with $u'_{f_{s1}}/U_j$ as low as 2%. Note that the condition $x_{s1} = 2x_{ex}$ stated by Monkewitz[28] to lead to the optimal aeroacoustic organisation of the pairing cascade, is not satisfied in this case. The successive pairings of vortices is then stopped downstream of the first pairing and $u'_{f_{s1}}$ does not display other maxima due to the absence of second subharmonic.

The coherence $C_{u'p'}(f_{s1})$ of the first subharmonic $u'_{f_{s1}}$ along the shear-layer was investigated by using a near field pressure signal $p'_{f_{s1}}$ as reference. The reference microphone was fixed in the vicinity of the jet at $r \simeq D/2, x = D/2$ and at an azimuthal angle of 90^o from the hot-wire traversed along the shear-layer. For $U_j = 20$ m.s^{-1}, $C_{u'p'}(f_{s1})$ is close to unity up to x_{s2} as shown in Figure 5. This indicates the absence of phase jitter between the velocity fluctuation $u'_{f_{s1}}$ and the generated near field pressure $p'_{f_{s1}}$. On the contrary, for $U_j = 40$ m.s^{-1}, a lower level of coherence is measured upstream of the pairing position x_{s1}. As shown by Hussain & Zaman,[21] ring vortices are indeed easily destabilized by random perturbations in the shear-layer, leading to the formation of circumferential lobe structures. This might result in the presence of phase jitter between the aerodynamic field and the acoustic field separated by an azimuthal angle of 90^o . The coherence $C_{u'p'}(f_{s1})$ collapses downstream of the pairing–breakdown location x_{s1}.

B. Acoustic radiation of the first subharmonic

Far-field pressure spectra, not shown here, indicate clearly the presence of the subharmonics of the excitation frequency, without frequency shift in function of the polar angle θ. These components are associated with the noise produced by fixed vortex pairings in the jet, as pointed out by Kibens,[10] Laufer & Yen[17] and Bridges & Hussain.[14] In the following, only the pressure field $p'_{f_{s1}}$ generated by the first vortex pairing process is considered.

In the present work, measurements of $p'_{f_{s1}}$ were made in the very close vicinity of the shear-layer by moving a microphone along the line $\theta = 10^o$ in order to follow the slow expansion of the jet. At the origin $x = 0$, the microphone is located at $D/5$ approximately from the shear-layer centre $r = D/2$. These data are reported in Figure 6(a) for the two jet velocities. For $U_j = 20$ m.s^{-1}, $|p'_{f_{s1}}|$ displays two strong maxima in x_{s1} and x_{s2}, close to the saturation of $u'_{f_{s1}}$ in the shear-layer center. This two-lobe distribution of the subharmonic pressure was also observed by Bridges & Hussain[14] as reported in their figure 10. Note that for $U_j = 40$ m.s^{-1}, the near pressure field is quite different.

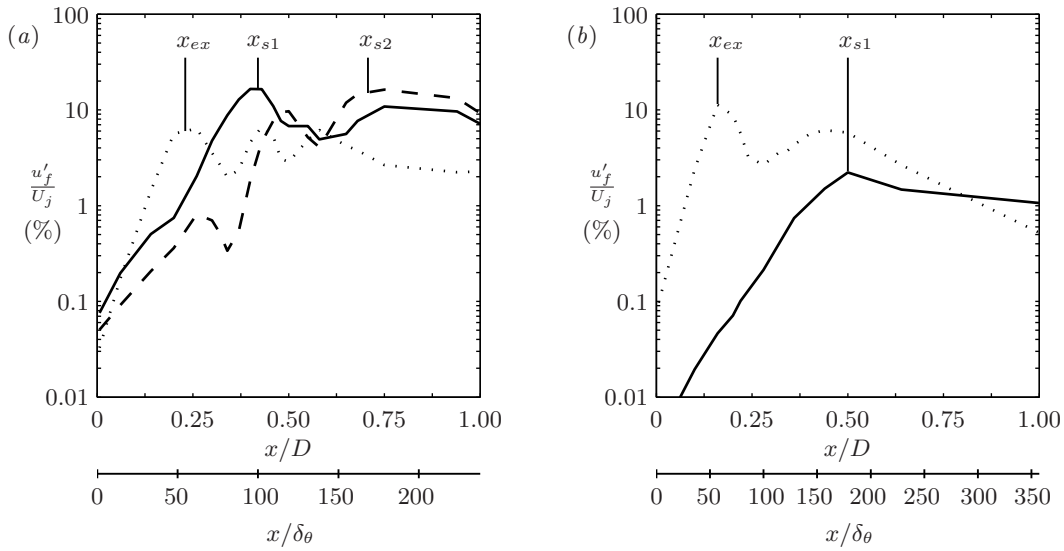

Figure 4. Growth of instability waves along the shear-layer centerline: (a) : $U_j = 20$ m.s^{-1} and (b) : $U_j = 40$ m.s^{-1}. The component associated to the excitation $u'_{f_{ex}}$ is represented by the dotted line ····· , $u'_{f_{s1}}$ by the solid line —— , and $u'_{f_{s2}}$ by the dashed line – – – .

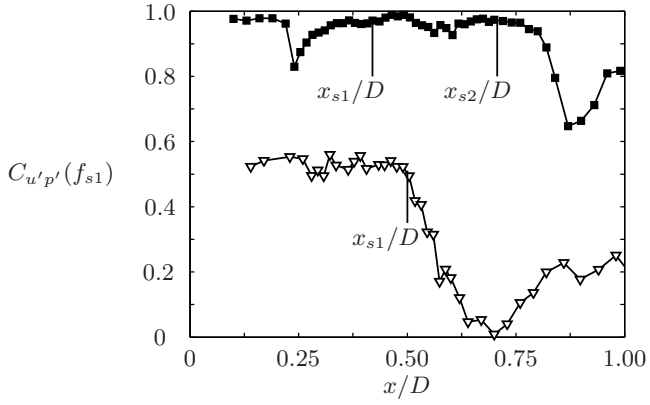

Figure 5. Correlation coefficient $C_{u'p'}(f_{s1})$ between the velocity fluctuation $u'_{f_{s1}}$ along the shear-layer and the pressure fluctuation $p'_{f_{s1}}$ in the jet vicinity. ■ : $U_j = 20$ m.s^{-1} and ▽ : $U_j = 40$ m.s^{-1}.

The acoustic directivity was also measured at 40 D from the nozzle exit as a function of the angle θ from the dowstream jet axis, and is shown in Figure 6(b). For the case $U_j = 20$ m.s^{-1}, the directivity presents a typical extinction angle that is often associated with the radiation of an axisymmetric quadrupolar source. For the case $U_j = 40$ m.s^{-1}, the radiation is strongly oriented in the downstream direction, with a dynamic of around 25 dB instead of the 15 dB found in the previous case.

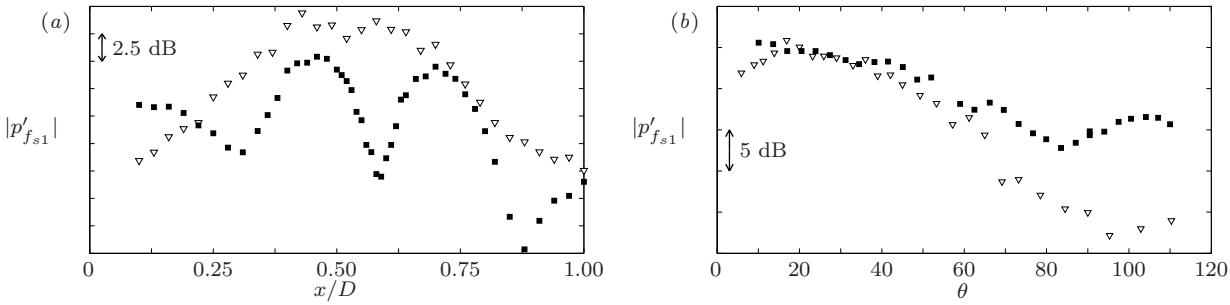

Figure 6. Distribution of the amplitude of the subharmonic pressure $p'_{f_{s1}}$: (a) along the shear-layer, (b) acoustic directivity. ■ : $U_j = 20$ m.s^{-1} and ▽ : $U_j = 40$ m.s^{-1}.

IV. Analysis based on a wavy-wall analogy

A. Acoustic directivity

Although the pairing is confined radially by the shear-layer thickness, its streamwise extent is comparable to the typical wavelength of $p'_{f_{s1}}$ in the near pressure field.[17] The global evolution of fluctuations along the shear-layer is then required for predicting the radiated acoustic field, as developed by Tam & Burton[29] to describe the Mach wave radiation by supersonic jets for instance. This approach was also used by Crighton & Huerre[19] to interpret the superdirective emission by vortex pairing observed in the experiments by Laufer & Yen.[17] These authors postulated the space-time evolution of the subharmonic pressure slightly outside the shear-layer to mimic the experimental results. This distribution has the form of a pressure wave convected in the downstream direction, and modulated by an envelope function $E(x)$:

$$p'_{f_{s1}} = E(x) \exp(ik_x x - i\omega t) \tag{1}$$

where k_x stands for the wavenumber and ω for the pulsation of the pairing.

In the present section, the wavy-wall model developed in Appendix A is applied with the near pressure field data as input, and the superdirective case is more specifically discussed. For the laminar case $U_j = 20$ m.s^{-1}, the near pressure field can be modelled with an analytical distribution based on sinusoidal functions :

$$E(x) \simeq \cos\left(\pi \frac{x - x_{s1}}{\sigma_e}\right) B(x, x_{s1}, \sigma_e) + P_{21} \cos\left(\pi \frac{x - x_{s2}}{\sigma_e}\right) B(x, x_{s2}, \sigma_e)$$

as shown in Figure 7(a). $B(x, x_{si}, \sigma_e)$ is the boxcar function, which is equal to one for $|x - x_{si}| < \sigma_e/2$ and zero otherwise. The parameter P_{21} is the ratio of the pressure amplitude between x_{s2} and x_{x1}, and σ_e refers to the length-scale of the envelope, taken to be the size of one sinusoidal arch. The expression (11) derived in Appendix A is then used to predict the acoustical directivity in the far field reported in Figure 7(b). All the parameters involved in the model are taken from the present experiments, and are reported in Table 3. For completeness, the analytical expression of the radiated pressure is given in Appendix B. The prediction approximates well the measurements and recovers a minimum pressure for $\theta = 90^o$. This value is basically controlled by the phase difference of the fluctuating pressure between the two lobes $k_x(x_{s2} - x_{s1})$, which is taken equal to π in the modeling and provides an exact cancellation in the crosswise direction $\theta = 90^o$.

The most interesting result is perhaps obtained for the transitional case $U_j = 40$ m.s^{-1}. The near pressure field can be fitted by functions defined from their Fourier transform (7) :

$$\hat{E}_n(k) = \exp\left[-(\sigma_n k)^n\right] \tag{2}$$

U_j	σ_e/D	λ_x/D	λ_∞/D	σ_e/λ_x	λ_∞/σ_e	M_p
20 m.s^{-1}	0.3	0.5	9.1	0.6	30.4	$0.9M_j$
40 m.s^{-1}	0.3	0.3	3.8	1.0	12.8	$0.7M_j$

Table 3. Parameters of the near and far pressure fields from measurements : σ_e is the length-scale of the enveloppe E, see expression (1), λ_x the wavelength of the oscillatory part, λ_∞ the acoustic wavelength and M_p the phase or convection Mach number, $M_p = \omega/k_x = \lambda_x/\lambda_\infty$.

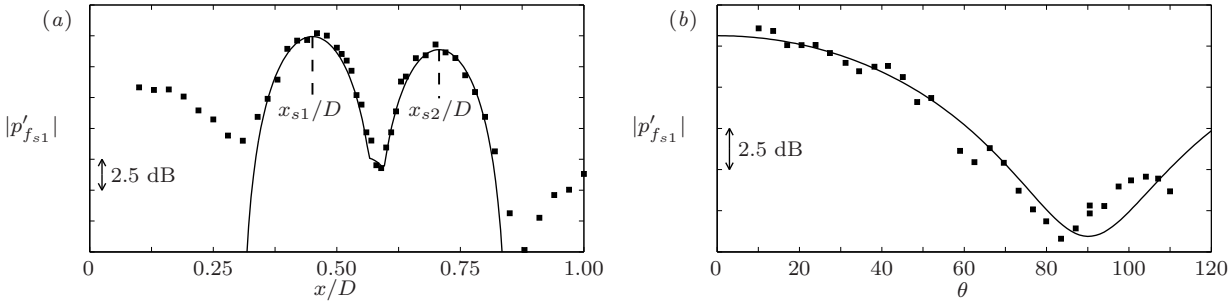

Figure 7. Laminar case ■ : $U_j = 20$ m.s^{-1}. (a) distribution of the amplitude of the subharmonic pressure $p'_{f_{s1}}$ along the shear-layer, and (b) acoustic directivity; —— analytical fit by sinusoidal distribution and associated directivity given by expression (11).

For $n = 2$, 3 or 4, comparisons with pressure measurements along the shear-layer are in good agreement, as shown in Figure 8(a). Note that the case $n = 2$ corresponds to the Gaussian distribution used by Crighton & Huerre[19] to derive an expression of the radiated acoustic field. By applying again the approach derived in Appendix A, the acoustic far-field associated with the distributions $E_n(x)$ is given by :

$$|p'_{f_{s1}}(R,\theta)| \propto \frac{1}{k_\infty R} \exp\left(n\sigma_n^n k_x^n \times M_p \cos\theta\right) \tag{3}$$

for $M_p \ll 1$, where M_p is the phase Mach number defined from (1) as $M_p = \omega/k_x$, see also Table 3. For the far field directivity, only the numerical factor varies with respect to the considered function E_n. The calculated directivities are plotted in Figure 8(b) and a good agreement is found with experimental data for the case $n = 3$, for which $n\sigma_n^n k_x^n|_{n=3} \simeq 45$. This result is also in agreement with the empirical expression derived by Laufer & Yen[17] in fitting their measurements, namely $|p'_{f_{s1}}| \propto \exp(45 \times M_p \cos\theta)$.

For $n = 4$, an attenuation coefficient $n\sigma_n^n k_x^n|_{n=4}$ of around 150 is found, which yields a directivity far sharper than the measurements. And the radiated acoustic field predicted by the model (11) for a Gaussian distribution provides a numerical factor $n\sigma_n^n k_x^n|_{n=2} \simeq 20$, and thus a poor approximation of the far-field pattern.

B. Near-field sound pressure

The decay of $p'_{f_{s1}}$ was investigated by moving the microphone away from the point $(x = D/2, r = D/2)$, and by following a fixed direction θ. The microphone displacement is denoted by d. For the two jet velocities, two directions were considered, $\theta = 90^o$ and $\theta = 20^o$. These measured profiles are compared to the incompressible limit of the wave-wall approach developed in Appendix A.

For $U_j = 20$ m.s^{-1}, the decay of $p'_{f_{s1}}$ very close to the shear-layer indicates a fast exponential evolution, with more than 40 dB of attenuation as shown in Figure 9(a). The agreement with the prediction (12) is fairly good in the vicinity of the shear-layer. A classical $1/d$ decay law is recovered farther away, for $d > 2D$ in the crosswise direction and for $d > 4D$ at $\theta = 20°$, as reported in Figure 9(b).

For $U_j = 40$ m.s^{-1}, the initial decay of $p'_{f_{s1}}$ is very similar and also indicates an exponential decay of 40 dB, see Figure 10, and the $1/d$ decay law is recovered for $d > 3D$. Favorable comparisons are obtained with $n = 3$ for the description of the boundary pressure. Note that the pressure decay associated with the Gaussian envelope function, $n = 2$, is not in good agreement with the experimental data.

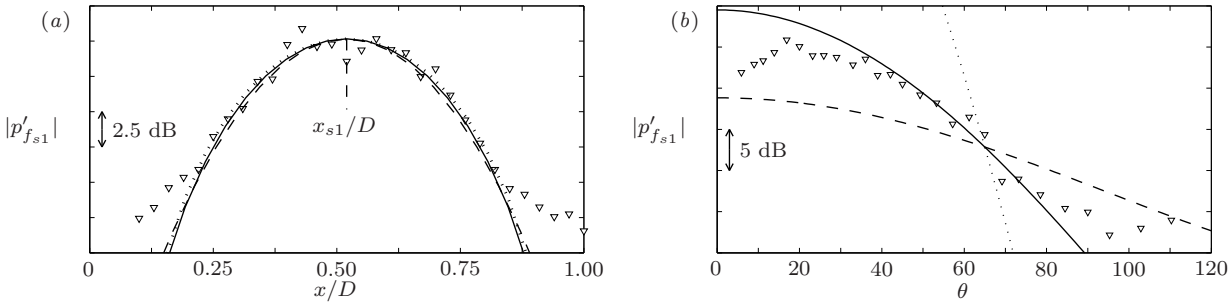

Figure 8. Transional case ▽ : $U_j = 40$ m.s^{-1}. (a) distribution of the amplitude of the subharmonic pressure $p'_{f_{s1}}$ along the shear-layer, and (b) acoustic directivity; analytical fit by E_n functions, see definition (2), with $n = 2$ --- (Gaussian), $n = 3$ —— , $n = 4$ ····· and associated directivity given by expression (11). The parameter σ_n involved in (1) is taken as $\sigma_2 = \sigma_e/2$ for $n = 2$, $\sigma_3 \simeq \sigma_4 \simeq 0.125D$ for $n = 3$ and 4.

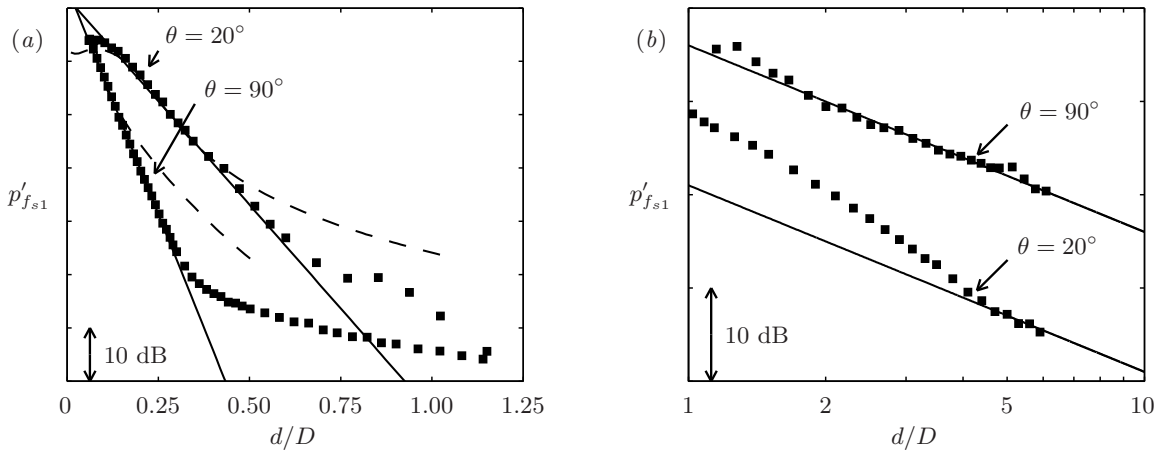

Figure 9. Laminar case ■ : $U_j = 20$ m.s^{-1}. Decay of the near pressure field $p'_{f_{s1}}$ in two directions $\theta = 20°$ and $\theta = 40°$: (a) in the vicinity of the shear-layer, --- incompressible wavy-wall analogy (12), —— exponential attenuation given by (4); (b) farther away from the shear-layer, —— $1/d$ decay law.

The radial attenuation of the near pressure field is not sensitive to the detailed streamwise distribution of $p'_{f_{s1}}$ along the shear-layer. This result can be emphasized with the expression (15) of the near pressure field for a slowly modulated boundary pressure $\sigma_e k_x \gg 1$, where σ_e is the characteristic length scale of the envelope E in (1). The near pressure decays exponentially according to the distance from the shear-layer centre $r - D/2$, with an attenuation rate based on k_x and with no influence of the form of the function $E(x)$. This asymptotic model describes fairly well our observations, but underestimates the decay rate found experimentally in the near-field. The following empirical expression is found to be more relevant :

$$|p'_{f_{s1}}| \propto \exp\left[-\alpha k_x (r - D/2)\right] \tag{4}$$

For $U_j = 40$ m.s^{-1}, the parameter α is around two, independently of the direction θ. For $U_j = 20$ m.s^{-1}, α varies slightly according to θ, and is equal to approximately $\alpha \simeq 3$ for $\theta = 90^o$ and $\alpha \simeq 4$ for $\theta = 20^o$.

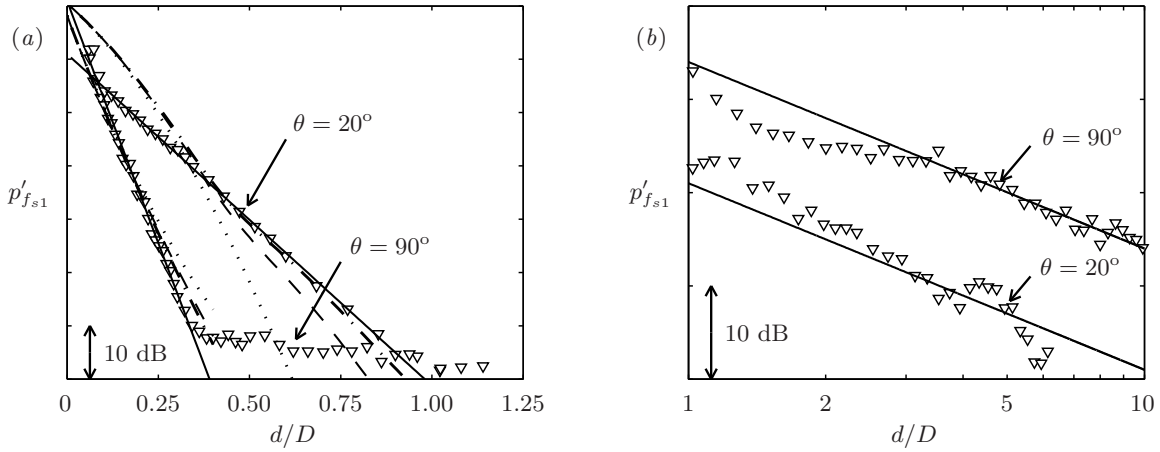

Figure 10. Transional case ▽ : $U_j = 40$ m.s^{-1}. Decay of the near pressure field $p'_{f_{s1}}$ in two directions $\theta = 20°$ and $\theta = 40°$: (a) in the vicinity of the shear-layer, – – – incompressible wavy-wall analogy (12) for $n = 3$, ····· $n = 2$ (Gaussian distribution), – · – · – $n = 4$, —— exponential attenuation given by (4); (b) farther away from the shear-layer, —— $1/d$ decay law.

V. Discussion and concluding remarks

In the present work, acoustic radiation generated by vortex pairings in a circular low-Mach-number excited jet has been investigated experimentally for two different initial states of the boundary layer at the nozzle exit. For a laminar boundary layer at the nozzle exit, a stable pairing cascade occurs and the noise radiated by the first subharmonic is close to the theoretical radiation of a compact axisymmetric source. A superdirective radiation has been observed for a transitional boundary layer, with a exponential directivity of the form $\sim \exp(\beta \times M_p \cos\theta)$. These two regimes have been reproduced for the first time in the same facility, and the present experimental work is the second experimental evidence of superdirective emission in jet noise since the work of Laufer & Yen.[17] Specific mechanisms for these two acoustic radiations have been found. In particular, the classical vortex pairing noise and the superdirective radiation have been distinguished according to the vortex dynamics, either stable and very well organized in the first case, or followed by vortex breakdown in the second case.

From a theoretical point of view, these two radiation patterns can be recovered from a wave extrapolation method, as developed in the present Appendix A in following the study of Crighton & Huerre.[19] Such an approach allows to understand the structure of the near acoustic field, and to identify the different involved length scales. Note that similar developments have also been proposed for the acoustic radiation of a Tollmien-Schlichting wave.[30,31] In the superdirective case, favorable comparisons with experiments are found for a near pressure defined from expression (2) with $n = 3$, and the pressure amplitude is then found as follows :

$$|p'_{f_{s1}}(R,\theta)| \propto \frac{1}{k_\infty R} \exp\left(\beta \times M_p \cos\theta\right) \qquad \beta \simeq 45$$

A possible next step could be to use the direct computation of aerodynamic noise[32] to reproduce these two configurations by controlling separately Reynolds and Mach numbers. Mean flow propagations effects would be included and would allow to discuss more precisely the presence and the location of an extinction angle for the far-field directivity.

Appendix

A. Acoustic radiation of an axisymmetric pressure distribution

The acoustic field radiated from an axisymmetric pressure distribution into a quiescent medium is investigated. The pressure is prescribed in $r = r_j = D/2$ as a traveling wave modulated by an envelope $E(x)$:

$$p'(x, r = r_j, t) = E(x) \exp\left[i(k_x x - \omega t)\right] \tag{5}$$

where ω and k_x are the pulsation and the axial wavenumber of the fluctuation respectively. The pressure $p'(x, r, t)$ in the domain $r \geq r_j$ is then sought as :

$$p'(x, r, t) = p(x, r) \exp(-i\omega t)$$

The pressure $p(x, r)$ is governed by the Helmholtz equation :

$$\left(\frac{\partial^2}{\partial x^2} + \frac{1}{r}\frac{\partial}{\partial r} + \frac{\partial^2}{\partial r^2}\right) p + k_\infty^2 p = 0 \tag{6}$$

with $k_\infty = \omega/c_\infty$ the acoustic wavenumber and c_∞ the speed of sound. By taking the Fourier transform of $p(x, r)$ according to x,

$$\widehat{p}(k, r) = \frac{1}{2\pi} \int_{-\infty}^{+\infty} p(x, r) \exp(-ikx) dx \tag{7}$$

the solution of the wave equation (6) is given by :

$$\widehat{p}(k, r) = \begin{cases} C(k) H_0^1(ik_r r) & \text{if} \quad |k| > k_\infty \\ C(k) H_0^1(k_r r) & \text{otherwise} \end{cases} \tag{8}$$

where $k_r = \sqrt{|k_\infty^2 - k^2|}$ is the transverse wavenumber and H_0^1 is the Hankel function of the first kind and zero order. The coefficient $C(k)$ is deduced by the Fourier transform of the boundary condition (5) :

$$C(k) = \begin{cases} \hat{E}(k - k_x)/H_0^1(ik_r r_j) & \text{if} \quad |k| > k_\infty \\ \hat{E}(k - k_x)/H_0^1(k_r r_j) & \text{otherwise} \end{cases} \tag{9}$$

The solution $p(x, r)$ to the problem (5) and (6) is then obtained by taking the inverse Fourier transform of $\hat{p}(k, r)$. In the following, asymptotic expressions of the pressure $p(x, r)$ in the far and near fields are derived.

Regarding the far field, *i.e.* for $k_r r \gg 1$, $|\hat{p}(k, r)|$ decays as $1/\sqrt{r}$ for $|k| < k_\infty$ and as $\exp(-k_r r)/\sqrt{r}$ for $|k| > k_\infty$. Thus, the contribution to the far acoustic field results mainly from components $|k| < k_\infty$ and the pressure $p(x, r)$ reduces to :

$$p(x, r) \sim \int_{-k_\infty}^{+k_\infty} \frac{\hat{E}(k - k_x)}{H_0^1(k_r r_j)} H_0^1(k_r r) \exp(ikx) dk$$

In order to estimate the directivity pattern, the polar coordinates (R, θ) are introduced for the observer. The method of stationary phase then yields, for $k_r R \cos\theta \gg 1$:

$$p'(R, \theta, t) \sim \sqrt{2\pi}\, \frac{k_\infty \hat{E}(k_\infty \cos\theta - k_x)}{H_0^1(k_\infty r_j \sin\theta)} \frac{\exp(ik_\infty R - i\omega t + i\pi/4)}{k_\infty R} \tag{10}$$

This expression can be further simplified by assuming the pressure field to be radially compact, *i.e.* $k_\infty r_j \ll 1$. The term $H_0^1(k_\infty r_j \sin\theta)$ can thus be approximated by $2i \ln(k_\infty r_j)/\pi$. In addition, by introducing

the Doppler factor $D_\theta = 1 - M_p \cos\theta$ where M_p is the phase Mach number defined as $M_p = k_\infty / k_x$, expression (10) can be expressed as :

$$p'(R,\theta,t) \sim \sqrt{\frac{\pi}{2}} \frac{\pi}{\ln(k_\infty r_j)} \times k_\infty \hat{E}(-k_x D_\theta) \times \frac{\exp(ik_\infty R - i\omega t - i\pi/4)}{k_\infty R} \tag{11}$$

This asymptotic expansion is relevant for the configurations investigated in this study, since $k_\infty r_j = 0.34$ for $U_j = 20$ m.s^{-1} and $k_\infty r_j = 0.83$ for $U_j = 40$ m.s^{-1}.

Regarding the near pressure field, *i.e.* for $k_\infty |r - r_j| \ll 1$, compressibility effects are negligible and the problem governed by equations (5) and (6) can be simplified by setting $k_\infty = 0$. The solution $\hat{p}(k,r)$ is then directly deduced from expressions (8) and (9) :

$$\hat{p}(k,r) = \frac{\hat{E}(k-k_x)}{H_0^1(i|k|r_j)} H_0^1(i|k|r)$$

and the near pressure field $p(x,r)$ is given by :

$$p(x,r) = \int_{-\infty}^{+\infty} \frac{\hat{E}(k-k_x)}{H_0^1(i|k|r_j)} H_0^1(i|k|r) \exp(ikx) dk \tag{12}$$

This expression of the near-field can be evaluated for a slowly spatially modulated boundary pressure (5), *i.e.* for $\sigma_e/\lambda_x \gg 1$ or $\sigma_e k_x \gg 1$, where σ_e is the typical length scale of the envelope $E(x)$ and $\lambda_x = 2\pi/k_x$ is the wavelength of the pressure wave. By splitting the integral (12) according to positive and negative k wavenumbers and by introducing the new variable $u = \sigma_e(k - k_x)$, the pressure $p(x,r)$ becomes :

$$\begin{aligned} p(x,r) = \exp(ik_x x) \int_{-\sigma_e k_x}^{+\infty} \frac{\hat{E}(u/\sigma_e)}{H_0^1\left[i(\sigma_e k_x + u)\frac{r_j}{\sigma_e}\right]} H_0^1\left[i(\sigma_e k_x + u)\frac{r}{\sigma_e}\right] \exp\left(i\frac{u}{\sigma_e}x\right)\frac{du}{\sigma_e} \\ + \exp(ik_x x) \int_{-\infty}^{-\sigma_e k_x} \frac{\hat{E}(u/\sigma_e)}{H_0^1\left[-i(\sigma_e k_x + u)\frac{r_j}{\sigma_e}\right]} H_0^1\left[-i(\sigma_e k_x + u)\frac{r}{\sigma_e}\right] \exp\left(i\frac{u}{\sigma_e}x\right)\frac{du}{\sigma_e} \end{aligned} \tag{13}$$

For $\sigma_e k_x \gg 1$, $p(x,r)$ is mainly given by the contribution of the first integral, which can be evaluated by expanding the two Hankel functions H_0^1. Hence :

$$p(x,r) \sim \exp(ik_x x) \int_{-\infty}^{+\infty} \hat{E}\left(\frac{u}{\sigma_e}\right) \frac{\exp(-(k_x + u/\sigma_e)r)/\sqrt{(k_x + u/\sigma_e)r}}{\exp(-(k_x + u/\sigma_e)r_j)/\sqrt{(k_x + u/\sigma_e)r_j}} \exp\left(i\frac{u}{\sigma_e}x\right)\frac{du}{\sigma_e}$$

By introducing the variable $z = x + i(r - r_j)$, the near pressure field reads :

$$p(x,r) \sim \sqrt{\frac{r_j}{r}} E(z) \exp(ik_x z) \tag{14}$$

The boundary pressure in $r = r_j$ is thus analytically continuated in the near-field $r \geq r_j$, with a supplementary attenuation factor in $1/\sqrt{r}$. A cruder expansion can be obtained by comparing the characteristic length-scales of the evolution of $E(z)$, $(r_j/r)^{1/2}$ and $\exp(ik_x z)$ for $\sigma_e k_x \gg 1$. For this, expression (14) is written according to the auxiliary variable $\eta = k_x z$:

$$p(x,r) \sim \sqrt{\frac{r_j}{r_j + \Im(\sigma_e \eta)/(\sigma_e k_x)}} E\left(\frac{1}{\sigma_e k_x}\sigma_e \eta\right) \exp(i\eta)$$

and for $\sigma_e k_x \gg 1$, one obtains:

$$p(x,r) \sim E(0)\ \exp(ik_x z)$$

Finally, $|p(x,r)|$ reduces to the exponential evolution :

$$|p(x,r)| \propto \exp\left[-k_x(r - r_j)\right] \tag{15}$$

To sum up, expression (11) provides the acoustic far field for any boundary pressure (5), and in particular, regardless of its axial compacity $\sigma_e k_x$. Only the condition $k_\infty r_j \ll 1$ has been assumed. For comparison, the expression found by Crighton & Huerre,[19] see their equation (3.4), for the acoustic field generated by a plane boundary pressure is recalled with our notations :

$$p(R,\theta,t) \sim \sqrt{2\pi}\, \sin\theta\, k_\infty \hat{E}(k_\infty \cos\theta - k_x) \times \frac{\exp\left(ik_\infty R - i\omega t - i\frac{\pi}{4}\right)}{\sqrt{k_\infty R}}$$

The main differences with expression (11) are the $1/\sqrt{R}$ decay law and the dipolar term in $\sin\theta$ due to the two-dimensional geometry of the problem considered by Crighton & Huerre[19].[19] Note also that the behaviour of the near pressure field can be also estimated by (15) in assuming a slowly modulated boundary pressure for (5), *i.e.* $\sigma_e/\lambda_x \gg 1$.

B. Application to the laminar case $U_j = 20$ m.s^{-1}

The experimental near pressure field displayed in Figure 7(a), is represented by :

$$E(x) = \cos\left(\pi \frac{x - x_{s1}}{\sigma_e}\right) B(x, x_{s1}, \sigma_e) + P_{21} \cos\left(\pi \frac{x - x_{s2}}{\sigma_e}\right) B(x, x_{s2}, \sigma_e) \tag{16}$$

To estimate the acoustic directivity, the Fourier transform $\hat{E}(x)$ of the sinusoidal distribution (16) must be evaluated :

$$\hat{E}(k) = \{\exp(ikx_{s1}) + P_{21}\exp(ikx_{s2})\} \frac{\cos\left(\frac{k\sigma_e}{2}\right)}{1 - \left(\frac{k\sigma_e}{\pi}\right)^2}$$

and the acoustic directivity is then explicitly provided by expression (11) :

$$|p'(R,\theta)| \propto \frac{\pi^{3/2}}{\sqrt{2}} \frac{k_{ac}\sigma_e}{\ln(k_{ac} r_j)} \frac{1}{k_{ac} R} I(\theta) D_a(\theta) \tag{17}$$

The Factor $D_a(\theta)$ is the directivity associated to a single sinusoidal arch centered in $x = 0$:

$$D_a(\theta) = \left| \frac{\cos\left(\frac{k_x\sigma_e}{2} D_\theta\right)}{1 - \left(\frac{k_x\sigma_e}{\pi}\right)^2 D_\theta^2} \right|$$

and $I(\theta)$ accounts for the interference between the acoustic waves emitted from the two arches :

$$I(\theta) = |\exp(ik_x x_{s1} D_\theta) + P_{21}\exp(ik_x x_{s2} D_\theta)|$$

where $D_\theta = 1 - M_p \cos\theta$ corresponds to the Doppler factor. The results plotted in Figure 7(b) are obtained with the numerical values given in Table 3, and with $P_{21} = 0.957$.

References

[1]Mollo-Christensen, E., Kolpin, M.A. & Martucelli, J.R., 1964, Experiments on jet flows and jet noise far-field spectra and directivity patterns, *J. Fluid Mech.*, Vol. 18, pp. 285-301.

[2]Crow, S.C. & Champagne, F.H., 1971, Orderly structure in jet turbulence, *J. Fluid Mech.*, Vol. 48, No. 3, pp. 547-591.

[3]Laufer, J., Kaplan, R.E. & Chu, W.T., 1974, On the noise generation of jet noise, *AGARD CP-131 Noise Mechanisms*, pp. 21-1 to 21-7.

[4]Mitchell, B.E., Lele, S.K. & Moin, P., 1999, Direct computation of the sound generated by vortex pairing in an axisymmetric jet, *J. Fluid Mech.*, Vol. 383, pp. 113-142.

[5]Bastin, F., Lafon, P. & Candel, S., 1997, Computation of jet mixing noise due to coherent structures: the plane jet case, *J. Fluid Mech.*, Vol. 335, pp. 261-304.

[6]Bogey, C., Bailly, C. & Juvé, D., 2000, Numerical simulation of the sound generated by vortex pairing in a mixing layer, *AIAA Journal*, Vol. 38, No. 12, pp. 2210-2218.

[7]Huerre, P. & Crighton, D.G., 1983, Sound generation by instability waves in a low Mach number jet, *AIAA 8th Aeroacoustics conference*, Atlanta, Georgia, AIAA Paper 83-0661.

[8]Bridges, J.E., 1990, Application of coherent structure and vortex sound theories to jet noise, *Ph. D. Thesis*, University of Houston.

[9]Schram, C., Taubitz, S., Anthoine, J. & Hirschberg, A., 2005, Theoretical/empirical prediction and measurement of the sound produced by vortex pairing in a low Mach number jet, *J. Sound Vib.*, Vol. 181, pp. 171-187.

[10]Kibens, V., 1979, Discrete noise spectrum generated by an acoustically excited jet, *AIAA Journal*, Vol. 18, No. 4, pp. 434-441.

[11]Zaman, K.B.M.Q. & Hussain, A.K.M.F., 1980, Vortex pairing in a circular jet under controlled excitation. Part 1. general response, *J. Fluid Mech.*, Vol. 101, pp. 449-491.

[12]Michalke, A., 1965, On spatially growing disturbances in an inviscid shear layer, *J. Fluid Mech.*, Vol. 23, No. 3, pp. 521-544.

[13]Freymuth, P., 1966, On transition in a separated laminar boundary layer, *J. Fluid Mech.*, Vol. 25, No. 4, pp. 683-704.

[14]Bridges, J. & Hussain, F., 1992, Direct evaluation of aeroacoustic theory in a jet, *J. Fluid Mech.*, Vol. 240, pp. 469-501.

[15]Möhring, W., 1978, On vortex sound at low Mach number, *J. Fluid Mech.*, Vol. 85, No. 4, pp. 685-691.

[16]Kambe, T. & Minota, T., 1983, Acoustic wave radiation by head-on collision of two vortex rings, *Proc. R. Soc. Lond.*, A 386, pp. 277-308.

[17]Laufer, J. & Yen, T.C., 1983, Noise generation by a low Mach number jet, *J. Fluid Mech.*, Vol. 134, pp. 1-31.

[18]Zaman, K.B.M.Q., 1985, Far-field noise of a subsonic jet under controlled excitation, *J. Fluid Mech.*, Vol. 152, pp. 83-111.

[19]Crighton, D.G. & Huerre, P., 1990, Shear-layer pressure fluctuations and superdirective acoustic sources, *J. Fluid Mech.*, Vol. 220, pp. 355-368.

[20]Lighthill, M.J., 1952, On sound generated aerodynamically - I. General theory, *Proc. Roy. Soc. London*, Vol. 211, Ser. A, 1107, pp. 564-587.

[21]Hussain, A.K.M.F. & Zaman, K.B.M., 1980, Vortex pairing in a circular jet uner controlled excitation. Part 2. coherent structure dynamics, *J. Fluid Mech.*, Vol. 101, pp. 493-544.

[22]Berhault, J.P., Sunyach, M., Arbey, H. & Comte-Bellot, G., 1973, Réalisation d'une chambre anéchoïque revêtue de panneaux et destinée à l'étude des bruits d'origine aérodynamique (in french), *Acustica*, Vol. 29, No. 2, pp. 69-78.

[23]Fleury, V., 2006, Superdirectivité, bruit d'appariement et autres contributions au bruit de jet (in french), *Ph.D. Thesis*, Ecole Centrale de Lyon, 2006-xx.

[24]Husain, H.S. & Hussain, A.K.M.F., 1995, Experiments on subharmonic resonance in a shear layer, *J. Fluid Mech.*, Vol. 304, pp. 343-372.

[25]Monkewitz, P.A. & Sohn, K.D., 1988, Absolute instability in hot jets, *AIAA Journal*, Vol. 26, No. 8, pp. 911-916.

[26]Ho, C.M. & Huang, L.S., 1982, Subharmonics and vortex merging in mixing layers, *J. Fluid Mech.*, Vol. 119, pp. 443-473.

[27]Laufer, J. & Zhang, J.X., 1983, Unsteady aspects of a low Mach number jet, *Phys. Fluids*, Vol. 26, No. 7, pp. 1740-1750.

[28]Monkewitz, P.A., 1983, On the nature of the amplitude modulation of jet shear layer instability waves, *Phys. Fluids*, Vol. 26, No. 11, pp. 3180-3184.

[29]Tam, C.K.W. & Burton, D.E., 1984, Sound generated by instability waves of supersonic flows. Part 2: axisymmetric jets, *J. Fluid Mech.*, Vol. 138, pp. 273-295.

[30]Akylas, T.R. & Toplosky, N., 1986, The sound field of a Tollmien-Schlichting wave, *Phys. Fluids*, Vol. 29, No. 3, pp. 685-689.

[31]Wu, X. & Hogg, L.W., 2006, Acoustic radiation of Tollmien-Schlichting waves as they undergo rapid distorsion, *J. Fluid Mech.*, Vol. 550, pp. 307-347.

[32]Bogey, C. & Bailly, C., 2006, Investigation of downstream and sideline subsonic jet noise using Large Eddy Simulations, *Theoretical and Computational Fluid Dynamics*, Vol. 20, No. 1, pp. 23-40.